This is the accepted manuscript made available via CHORUS. The article has been published as:

Parametric Frequency Divider Based Ising Machines

Nicolas Casilli, Tahmid Kaisar, Luca Colombo, Siddhartha Ghosh, Philip X.-L. Feng, and Cristian Cassella

Phys. Rev. Lett. **132**, 147301 — Published 2 April 2024

DOI: 10.1103/PhysRevLett.132.147301

Parametric Frequency Divider based Ising Machines

Nicolas Casilli[1],* Tahmid Kaisar[2],* Luca Colombo[1], Siddhartha Ghosh[1], Philip X.-L. Feng[2],† and Cristian Cassella[1‡]
[1]*Department of Electrical and Computer Engineering, Northeastern University, Boston, MA 02115, USA and*
[2]*Department of Electrical and Computer Engineering, University of Florida, Gainesville, FL 32611, USA*
(Dated: February 21, 2024)

We report on a new class of Ising machines (IMs) that rely on coupled parametric frequency dividers (PFDs) as macroscopic artificial spins. Unlike the IM counterparts based on subharmonic-injection locking (SHIL), PFD IMs do not require strong injected continuous-wave signals or applied DC voltages. Therefore, they show a significantly lower power consumption per spin compared to SHIL-based IMs, making it feasible to accurately solve large-scale combinatorial optimization problems (COPs) that are hard or even impossible to solve by using the current von Neumann computing architectures. Furthermore, using high quality (Q) factor resonators in the PFD design makes PFD IMs able to exhibit a nanoWatt-level power-per-spin. Also, it remarkably allows a speed-up of the phase synchronization among the PFDs, resulting in shorter time-to-solution and lower energy-to-solution despite the resonators' longer relaxation time. As a proof of concept, a 4-node PFD IM has been demonstrated. This IM correctly solves a set of Max-Cut problems while consuming just 600 nanoWatts per-spin. This power consumption is two orders of magnitude lower than the power-per-spin of state-of-the-art SHIL-based IMs operating at the same frequency.

Owing to the well-known von Neumann bottleneck [1], most current computing architectures provide limited capability to efficiently solve large-scale nondeterministic polynomial-time (NP) hard problems within a reasonable amount of time [2]. To address this limitation, a new approach to solving NP-hard problems has emerged in the form of hardware solvers called Ising machines (IMs). An IM can be defined as a network of *artificial* spins [3], arranged and interconnected according to the problem at hand. This machine can accurately solve a combinatorial optimization problem (COP) by identifying the spin-state configuration that minimizes the corresponding Ising Hamiltonian [4–6]. Several systems have been developed in recent years to perform an efficient minimization of the Ising Hamiltonian, including: D-Wave systems [7–9], Coherent Ising machines (CIMs) [10–12], photonic IMs [13–15], SRAM-based IMs [16, 17], GPU-based IMs [18], and oscillator-based Ising machines (OIMs) [19–27]. D-Wave systems rely on superconducting devices [7] requiring cryogenic operating temperatures near zero kelvin to function properly. Consequently, they are bulky and consume a considerable amount of power due to the necessity of cryogenic refrigeration [8]. CIMs utilize fiber-based optical parametric oscillators [11, 12] to generate the spins and field-programmable-gate-arrays (FPGAs) to digitize the spins' coupling [10, 11]. As a result, they are also hardly usable when targeting a small form-factor and a low power consumption. Alternative photonic IMs based on spatial light modulation [13] or recurrent Ising sampling [14] have also been reported, showing promise for solving large-scale COPs. However, relying on these solvers also comes with challenges, primarily related to unfavorable times-to-solution caused by the required intense signal processing [15]. SRAM-based and

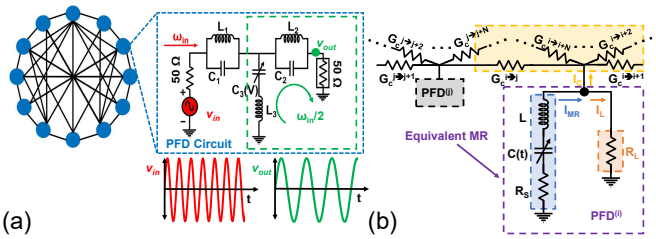


FIG. 1. a) Schematic view of a PFD IM; b) Schematic view of a network of coupled PFDs, where each PFD is described by an electrical Mathieu resonator (MR).

GPU-based IMs are digital hardware implementations of the simulated annealing algorithm or of one of its variants [4, 22]. These IMs can be manufactured using the same complementary metal-oxide-semiconductor (CMOS) fabrication processes [9] utilized for mass production of the integrated circuits in consumer electronics, offering significant benefits in terms of production cost, reprogrammability, and form-factor. However, the performance of these IMs depends on the problem being solved and can be significantly degraded for problems requiring heavy sequential computation [16–18, 21, 28]. For these reasons, the pursuit of highly miniaturized and low-power IMs has recently shifted towards OIMs, whose physics-inspired processing enables a higher degree of parallelism during the computation compared to digital solvers [17, 28].

OIMs leverage the collective dynamics of networks of bistable coupled electronic oscillators to perform the computation in an analog fashion. Among the demonstrated OIMs [4], those using "parametrons" as spins were the first ones to be proposed [29–32]. Parametrons attain phase bistability by triggering a

parametric oscillation in a circuit composed of one nonlinear resonator. In this regard, the dynamics of coupled parametric oscillators have been studied in the last few years to benchmark the computing performance achievable by CIMs and by parametron based IMs [29, 32, 33]. Yet, a full investigation of the accuracy of the retrieved problem solution when using an annealing schedule or when relying on resonant devices with high quality factor (Q), like the micro and nano photonic and electromechanical resonators available today [34–37], is currently missing. Moreover, all the reported parametrons require hundreds of milliWatts of input power to activate their oscillation. Such a high power consumption motivates why no attempt has ever been made to build large-scale electronic IMs based on parametrons (see Supplemental Material Section S3.3 for more information about the parametrons developed to date [38]). On the other hand, OIMs utilizing subharmonic-injection-locked (SHIL) oscillators as spins have garnered significant attention in recent years [19–25]. In these OIMs, dubbed here as "SHIL IMs", an artificial spin is represented by the bistable phase of a SHIL oscillator's output signal, which can be shifted by either 0 or π with respect to the output phase of a reference oscillator. SHIL IMs are generally analyzed by using the Kuramoto model [39], which only considers the phase of the SHIL oscillators' output signal and not the amplitude. The power consumed by each oscillator in SHIL IMs is typically in the hundreds of μWatts-range due to the need to sustain the oscillation, trigger the injection-locking regime, and synthesize the spin-coupling [4, 22]. As a result, the current SHIL IMs are also not easily scalable to solve realistically sized NP-hard problems while maintaining a low power consumption [4, 19, 20].

In this Letter, we present a class of OIMs referred to as parametric frequency divider based IMs (PFD IMs). In recent years, PFDs have been used for sensing [40, 41], signal processing [42, 43], and frequency generation [44, 45]. Like the previously reported parametrons, PFDs rely on a nonlinear reactance, such as a diode or a varactor, to passively activate a parametric oscillation at half of their driving signal's frequency (ω_0) when the input power levels exceed a certain threshold (P_{th}). Yet, in order to do so, they couple a set of four harmonically related resonances to boost the effectiveness of the parametric modulation in their circuit, thereby enabling P_{th} values that are orders of magnitude lower than previously demonstrated for parametrons [46, 47].

As depicted in Fig. 1-a, a PFD can be characterized as a two-port electrical network formed by two circuit meshes interconnected through a shunt branch that contains the nonlinear capacitor. The input mesh is driven by the PFD's input signal [$v_{in}(t)$], which modulates the capacitance of the nonlinear capacitor at an angular frequency ω_{in}. Each mesh incorporates a set of notch filters. These filters constrain $v_{in}(t)$ and the output signal, $v_{out}(t)$, within the PFD's input and output meshes respectively, allowing to analyze the PFD's behavior at each frequency by examining just one mesh. As described in [46], the reactive components in the output mesh of a PFD are selected to series-resonate at half of the input natural frequency (e.g., ω_{in}=$2\omega_0$) when neglecting the capacitance modulation induced by $v_{in}(t)$. This permits a mapping of the PFD's operation at or near ω_0 with only one second-order differential equation describing the voltage across the nonlinear capacitor. This mapping is equivalent to an electrical realization of a Mathieu resonator (*MR*, see Fig. 1-b) [48]. Such an *MR* has a Q equal to $1/(2\gamma_{tot})$, where γ_{tot} models the resonator's damping (e.g., γ_{tot}=$\omega_0 C_{av} R_{tot}/2$, where C_{av} is the average capacitance of the nonlinear capacitor for $v_{in}(t)$=0). R_{tot} is equal to R_L+R_s, where R_s denotes the *intrinsic* losses in the resonant system (e.g., the total resistance in the PFD's output mesh, R, combined with the resistance, R_d, capturing the Ohmic losses in the nonlinear capacitor's electrodes and dielectric film). Also, the *MR* has a resonance angular frequency in the absence of modulation equal to ω_0, and this frequency is periodically varied at a rate equal to ω_{in}. In this regard, we denote the magnitude of the resonance frequency modulation caused by the input signal at ω_{in} as p. As in its mechanical counterpart, the *MR* describing the operation of a single PFD enters a period-doubling regime for p-values larger than a certain threshold (p_{th}) equal to $4\gamma_{tot}$. More information on the *MR*-model of a PFD is provided in Supplemental Material Section S1 [38].

In order to demonstrate that networks of PFDs can be used as IMs, we analyze their interacting dynamics when they are coupled. This can be done by considering a number (N) of *MRs* with the same Q and ω_0 values, and we assume all couplings among the *MR*s to be purely dissipative (e.g., the PFDs are coupled through resistors connected to their output meshes). To this end, small coupling conductances ($\epsilon G_{i,j}$) with generic indices i and j can be used to map the interaction between the generic i-th and j-th *MRs*, as shown in Fig. 1-b. In particular, a summation can be used to capture all the interactions that any given *MR* is subject to based on the targeted problem to solve (see Supplemental Material Section S2 [38]). As an example, we report in Eq. (1) the *MR*-equation we have used to analyze the dynamics of the i-th *MR* during our analytical treatment. The variables $v_{i,j}$ in Eq. (1) describe the voltage across the nonlinear capacitors in the i-th and j-th *MRs*, respectively.

$$\ddot{v_i} + 2\epsilon\gamma_{tot}\omega_0\dot{v_i} + \omega_{out}^2 v_i + 2\gamma_L\omega_0 R_L \sum_{j\neq i} \epsilon G_{ij}\dot{v_j} = 0. \quad (1)$$

Differently from the equation of motion of only one

PFD (Supplemental Material Section S1 [38]), Eq. (1) includes an additional damping parameter, γ_L, equal to $\omega_0 C_{av} R_L/2$. Also, the angular resonance frequency for all *MR*s incorporates a "pump-depletion" term proportional to β [Eq. (2)] that is responsible for the saturation of the voltage across their nonlinear capacitors for $p{>}p_{th}$.

$$\omega_{out}^2 = \omega_0^2[1 + \epsilon p(1 - \beta(v_i)^2)\sin(2\omega_0 t)]. \tag{2}$$

It is important to point out that in Eqs. (1)-(2) both p and γ_{tot} are assumed to be small and are consequently scaled by a small parameter ϵ. From Eqs. (1)-(2), we can apply the Multiple Scales Method [49, 50] to derive a system of first-order differential equations [Eq. (3)] governing the dynamics of the complex voltage amplitude for the slow time scale $\tau{=}\epsilon t$. For the derivation of Eq. (3), we have assumed the lowest order response of v_i to be expressible as $B_i(\tau)e^{i\omega_0 t}{+}B_i^*(\tau)e^{-i\omega_0 t}$, where $B_i^*(\tau)$ is the complex conjugate of $B_i(\tau)$. Also, when *MR*s are used to solve a COP, we expect the solution to be encoded in the phase $[\phi(\tau)]$ of the complex amplitude reached at steady state by all the adopted *MR*s, similarly to what happens in CIMs and SHIL IMs. Therefore, from the real $[B_{i,re}(\tau)]$ and imaginary $[B_{i,im}(\tau)]$ parts of $B_i(\tau)$ we can calculate $\phi_i(\tau)$ as $\arctan[B_{i,im}(\tau)/B_{i,re}(\tau)]$. We then evaluate the steady-state value (Φ_i) of $\phi_i(\tau)$, and the same procedure is run for all the adopted *MR*s. Independently of the problem that needs to be solved, each *MR* can only reach two Φ-values, namely 0 or π, giving each PFD in a PFD IM the ability to passively emulate the dynamics of an Ising spin. In this regard, similar to CIMs, that utilize parametric dynamics to achieve phase bistability in the optical domain, the ground state solution identified by a PFD IM is governed by the minimization of a Lyapunov function considering both amplitude and phase dynamics [51, 52]. This computational principle is also similar to that of SHIL IMs, with the key distinction that the Lyapunov function governing SHIL IMs considers only the system's phase dynamics [22, 52]. More information about the dynamics of coupled PFDs are provided in Supplemental Material Section S4 [38].

$$\begin{aligned} B_i'(\tau) = \frac{1}{4}[(p\omega_0\beta)(B_i^3{-}3B_i{B_i^*}^2) + p\omega_0 B_i^* - \\ 4\omega_0 B_i\gamma_{tot} - 4\omega_0 R_L\gamma_L\sum_{j\neq i} G_{ij}B_j]. \end{aligned} \tag{3}$$

Starting from Eq. (3) (see Supplemental Material Section S2 [38]), we can evaluate the performance of a PFD IM when computing the solution of a COP over N variables, with each variable mapped to a specific PFD. In this regard, the performance of IMs are assessed based on several factors, including the probability of achieving a spin configuration that matches or closely matches the problem solution [i.e., the "probability-of-success" (P)], the time required to obtain a solution [i.e., the "time-to-solution" (T_S)], the power consumption of each spin [i.e., the "power-per-spin" (PW_{spin})], and the energy consumed by the entire machine during the computation [i.e., the "energy-to-solution" (E_S)]. In order to evaluate these computing performance metrics for PFD IMs, we construct a specific coupling matrix $[G]$ for each problem, with dimension $N{\times}N$. Each row of $[G]$ incorporates the conductance used to couple one specific PFD to any other PFDs. For each PFD, the phase of the slow complex amplitude [Eq. (3)] of its corresponding equivalent *MR* equation is numerically computed to obtain Φ. Then, P is determined based on a desired accuracy level (A). A is the minimum tolerated accuracy for the problem solution and its value ranges from 0 to 100%. Depending on whether we are looking at the probability to reach the ground-state (e.g., the global minimum for the targeted COP that identifies a 100% accurate solution) or at the probability to reach a close enough solution to the ground-state, with an accuracy higher than A but lower than 100%, P can be re-written as P_{GS} or P_A, respectively. Both P_{GS} and P_A can be computed for any targeted problem by solving it multiple times. After determining P_A, T_S can be calculated as [4]:

$$T_S = \tau_\phi \times [log_{(1-P_A)}(A)], \tag{4}$$

where τ_ϕ is the time that it takes on average for the phases of the slow-complex amplitudes of all coupled *MR*s to reach their final value when multiple problem-runs are executed. It is worth mentioning that the achievement of optimal computing performance can pass through the adoption of an annealing step, similarly to prior SHIL IMs [19]. To this end, p is gradually increased up to $1.005p_{th}$ from an initial value equal to $0.995p_{th}$ following an exponential trend [e.g., $p(t) = p_{th}(0.995{+}0.01(1{-}e^{-t/\tau_{ann}}))$, where τ_{ann} is the annealing rate and t is the time]. After determining T_S, bearing in mind that p reflects the voltage magnitude at ω_{in} across the varactor in each PFD and that P_{th} is proportional to p_{th}^2, we can estimate E_S for any problem as $NP_{th}\int_0^{T_S}(0.995 + 0.01(1 - e^{-t/\tau_{ann}}))^2\,dt$ [19, 21]. The P_{th} value considered during the computation of E_S can be directly found through a circuit simulation of a PFD (Supplemental Material Section S3 [38]). It is also worth mentioning that the ability to passively generate Ising dynamics without active components allows us to consider the Johnson noise generated by the *MRs*' resistors as the only noise process affecting the *MRs*' circuit [53].

To analyze and benchmark the performance of our PFD IMs, we choose to connect all the PFDs in a Möbius ladder configuration and to solve a set of unweighted Max-Cut problems of varying sizes [4, 7, 19]. COPs with a Möbius ladder graph are considered low-

complexity sparse problems [54]. Consequently, their correct solution can be numerically calculated, allowing to easily verify whether the solution found by a PFD IM is correct and, if it is not correct, to evaluate the difference in the computed number of cuts with respect to the expected value [6]. The number of cuts computed by a PFD IM is equivalent to the total number of paths of the problem-graph connecting PFDs with different output phases [6, 25].

By relying on our analytical model, we first investigated P_A, T_S and E_S when scaling N in the graph from 40 to 400 and when assuming specific values of tolerated accuracy (A=100% and A=97.5%) frequently used for benchmarking IMs [28]. During this study, we initially considered a Q=50, which is approximately the same Q of the resonators used by the PFDs assembled in this work. Also, we assumed an $\omega_0=2\pi\times10^6$ rad/sec, which coincides with the output angular frequency of our assembled PFD IM. For each considered N value, we computed the problem solution 100 times. This allowed us to determine P_{GS} and $P_{97.5\%}$ (see Fig. 2-a), together with the number of cuts identified by each executed problem-run. We found that the likelihood of generating a 100% accurate solution rapidly decays with respect to N, which is in line with what is generally observed in other IMs [4, 9, 17, 19, 21, 29]. Nevertheless, PFD IMs retain a 100% likelihood of calculating a cut-size within 2.5% of the highest possible number of cuts. In addition, after identifying τ_ϕ, we computed T_S and E_S vs. N when assuming a 100% or a 97.5% accuracy (see Figs. 2-b,c). In this regard, during the calculation of E_S we assumed a P_{th} value (600 nW) matching what we simulated and measured in our experiments. Evidently, we found an E_S value of 135 μJ (3.3 μJ) when assuming a 100% (97.5%) minimum tolerated accuracy in the calculation of T_S.

Subsequently, we conducted a second study driven by the growing accessibility of high-Q chip-scale resonator technologies that can be manufactured using the same semiconductor processes employed for solid-state varactors and diodes [34–37, 55]. In particular, it is reasonable to question whether incorporating these resonators in place of the $L-C$ resonators currently

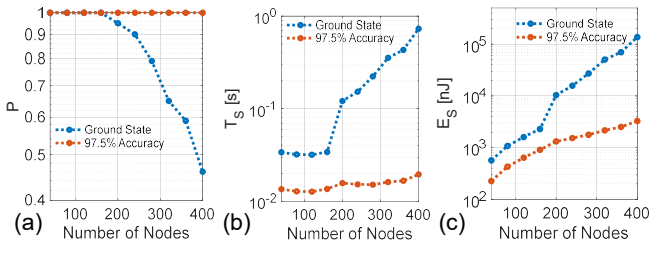


FIG. 2. Numerically computed trends of a) P_{GS} and $P_{97.5\%}$, b) T_S for A=97.5% or A=100%, and c) E_S for A=97.5% or A=100% vs. increasing N in Möbius ladder problems when τ_{ann} = 1 sec.

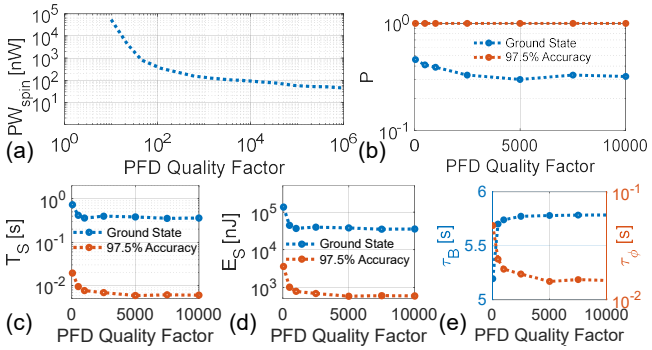


FIG. 3. Numerically computed trends for τ_{ann} = 1 sec vs. Q of a) PW_{spin}, b) P_{GS} and $P_{97.5\%}$, c) T_S when considering A=97.5% or A=100%, d) E_S when considering A=97.5% or A=100%, and e) τ_B and τ_ϕ.

used to construct PFDs could enhance the performance of PFD IMs. Therefore, we analyzed the performance of PFD IMs vs. Q. First, we calculated the trend (Fig. 3-a) of PW_{spin} vs. Q through a circuit simulator (see Supplemental Material Sections S3 and S5 [38]). Interestingly, we found that relying on resonators with Qs higher than 10^6 permits a reduction of PW_{spin} down to 60 nW, which is three orders of magnitude lower than the power required by each oscillator in state-of-the-art SHIL IMs. It is worth emphasizing that the saturation of PW_{spin} for Q values higher than 10^6 originates from the fact that R_L and R_d do not scale down with Q. We also analyzed P (Fig. 3-b), T_S (Fig. 3-c) and E_S (Fig. 3-d) vs. Q for a 400-node PFD IM solving the same Max-Cut problem we considered in Fig. 2 when assuming minimum tolerated accuracy levels of 100% and 97.5%, as in our first study. Interestingly, we found that relying on higher Q resonators does not change significantly the values of P_{GS} and $P_{97.5\%}$ with respect to the values found for a Q equal to 50 in Fig. 2. However, T_S reduces when assuming higher Q values, despite the fact that high-Q resonators inherently exhibit a longer relaxation time. This is due to the fact that τ_ϕ shortens when considering high Q values, even though a longer relaxation time (τ_B) is needed for the MRs to reach their steady-state amplitude (Fig. 3-e). Consequently, PFD IMs that rely on higher Q resonators inherently exhibit a lower E_S than their lower Q counterparts. As such, they are better suited for addressing COPs with a large number of variables. Finally, the impact of τ_{ann} on the computing performance of PFD IMs has also been analyzed for different N and Q values. We found that using a slower annealing rate when tackling large Möbius ladder problems remarkably leads to lower T_S and E_S values, despite the increase of τ_ϕ and independently of the MRs' Q value. We verified (Supplemental Material Section S5 [38]) that this improved performance can be attributed to a significant reduction in amplitude

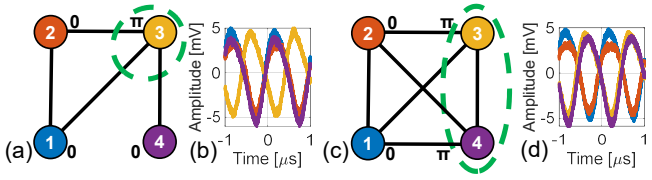


FIG. 4. a-d) Graphs and PFDs' output voltage waveforms relative to two Max-Cut problems tackled with the PFD IM built in this work.

heterogeneity for longer annealing rates [56, 57].

As a proof of concept, we built the first prototype of a PFD IM and we employed it to solve different unweighted Max-Cut problems, as in [19]. Four identical PFDs designed to work with a ω_{in} value of $4\pi*10^6$ rad/s were assembled on a printed-circuit-board (PCB) by using off-the-shelf inductors and capacitors to create resonant tanks with a Q value of nearly 50. Identical $2k\Omega$ coupling resistors, corresponding to 500 μS coupling conductances (Fig. 1-b), were used to couple the four PFDs according to the specific problem to solve. By running an electrical characterization of our PFDs, we were able to experimentally demonstrate a PW_{spin} value of 600 nW, which is the lowest one ever recorded for OIMs. It is worth emphasizing that all PFDs were designed to generate their subharmonic oscillation without requiring DC-voltages, thus without consuming any DC power for biasing the circuit. Fig. 4 shows the graphs of two of the nine Max-Cut problems investigated and solved by the PFD IM built in our experiments, together with the corresponding measured PFDs' output voltage. Evidently, the computed phase distribution matches the expected correct solution [19] for every problem we evaluated. A description of the experimental setup used during the testing of the assembled PFD IM is provided in Supplemental Material Section S6 [38], together with the graphs and output voltage waveforms for the other Max-Cut problems we have solved.

In conclusion, we have introduced PFD IMs and studied their computing performance when tackling various Möbius ladder problems with up to 400 nodes. Our findings suggest that incorporating high-Q resonators in the PFDs' design and using an annealing schedule allow to decrease PW_{spin} down to the nanoWatt-range, shorten T_S to less than 0.75 s, boost the P_{GS} up to 46% and achieve an E_S of 135 μJ for a 400-node Möbius ladder problem. We have also designed, built, and tested a prototype of a PFD IM that integrates four PFDs to solve several different Max-Cut problems. This prototype achieves a PW_{spin} of 600 nW by relying on off-the-shelf $L-C$ resonators with a Q near 50, and always retrieves the correct solutions for all the problems we have tackled. The demonstrated PW_{spin} is the lowest one ever reported for OIMs. Further investigation and performance evaluation will be required in the future to characterize the performance of PFD IMs for generic NP instances with densely connected graphs, beyond the Möbius ladder problems discussed in this Letter.

* N.C. and T.K. contributed equally to this publication.
† philip.feng@ufl.edu
‡ c.cassella@northeastern.edu

[1] J. Edwards and S. O'Keefe, Eager recirculating memory to alleviate the von Neumann Bottleneck, in *2016 IEEE Symposium Series on Computational Intelligence (SSCI)* (2016) pp. 1–5.
[2] F. Peper, The End of Moore's Law: Opportunities for Natural Computing?, New Gener. Comput. **35**, 253 (2017).
[3] F. Bohm, G. Verschaffelt, and G. V. der Sande, A poor man's coherent ising machine based on opto-electronic feedback systems for solving optimization problems, Nat Commun **10** (2019).
[4] N. Mohseni, P. L. McMahon, and T. Byrnes, Ising machines as hardware solvers of combinatorial optimization problems, Nat Rev Phys **4**, 363 (2022).
[5] A. Lucas, Ising formulations of many NP problems, Front. Physics **2**, 10.3389/fphy.2014.00005 (2014).
[6] K. P. Kalinin and N. G. Berloff, Computational complexity continuum within Ising formulation of NP problems, Commun Phys **5**, 20 (2022).
[7] R. Harris, J. Johansson, A. J. Berkley, M. W. Johnson, T. Lanting, S. Han, P. Bunyk, E. Ladizinsky, T. Oh, I. Perminov, E. Tolkacheva, S. Uchaikin, E. M. Chapple, C. Enderud, C. Rich, M. Thom, J. Wang, B. Wilson, and G. Rose, Experimental demonstration of a robust and scalable flux qubit, Phys. Rev. B **81**, 134510 (2010).
[8] M. W. Johnson, M. H. S. Amin, S. Gildert, T. Lanting, F. Hamze, N. Dickson, R. Harris, A. J. Berkley, J. Johansson, P. Bunyk, E. M. Chapple, C. Enderud, J. P. Hilton, K. Karimi, E. Ladizinsky, N. Ladizinsky, T. Oh, I. Perminov, C. Rich, M. C. Thom, E. Tolkacheva, C. J. S. Truncik, S. Uchaikin, J. Wang, B. Wilson, and G. Rose, Quantum annealing with manufactured spins, Nature **473**, 194 (2011).
[9] R. Afoakwa, Y. Zhang, U. K. R. Vengalam, Z. Ignjatovic, and M. Huang, CMOS Ising Machines with Coupled Bistable Nodes 10.48550/ARXIV.2007.06665 (2020).
[10] T. Inagaki, Y. Haribara, K. Igarashi, T. Sonobe, S. Tamate, T. Honjo, A. Marandi, P. L. McMahon, T. Umeki, K. Enbutsu, O. Tadanaga, H. Takenouchi, K. Aihara, K.-i. Kawarabayashi, K. Inoue, S. Utsunomiya, and H. Takesue, A coherent Ising machine for 2000-node optimization problems, Science **354**, 603 (2016).
[11] A. Marandi, Z. Wang, K. Takata, R. L. Byer, and Y. Yamamoto, Network of time-multiplexed optical parametric oscillators as a coherent Ising machine, Nature Photon **8**, 937 (2014).
[12] Q. Cen, H. Ding, T. Hao, S. Guan, Z. Qin, J. Lyu, W. Li, N. Zhu, K. Xu, Y. Dai, and M. Li, Large-scale coherent Ising machine based on optoelectronic parametric oscillator, Light Sci Appl **11**, 333 (2022).
[13] D. Pierangeli, G. Marcucci, and C. Conti, Large-scale

photonic ising machine by spatial light modulation, Phys. Rev. Lett. **122**, 213902 (2019).
[14] M. Prabhu, C. Roques-Carmes, Y. Shen, N. Harris, L. Jing, J. Carolan, R. Hamerly, T. Baehr-Jones, M. Hochberg, V. Čeperić, J. D. Joannopoulos, D. R. Englund, and M. Soljačić, Accelerating recurrent ising machines in photonic integrated circuits, Optica **7**, 551 (2020).
[15] H. Yamashita, K.-i. Okubo, S. Shimomura, Y. Ogura, J. Tanida, and H. Suzuki, Low-rank combinatorial optimization and statistical learning by spatial photonic ising machine, Phys. Rev. Lett. **131**, 063801 (2023).
[16] Y. Su, T. T.-H. Kim, and B. Kim, FlexSpin: A Scalable CMOS Ising Machine with 256 Flexible Spin Processing Elements for Solving Complex Combinatorial Optimization Problems, in *2022 IEEE International Solid- State Circuits Conference (ISSCC)* (IEEE, San Francisco, CA, USA, 2022) pp. 1–3.
[17] M. Yamaoka, *Overview of CMOS Annealing Machine*, Special Features (Research and Development Group, Hitachi, 2019).
[18] C. Cook, H. Zhao, T. Sato, M. Hiromoto, and S. X.-D. Tan, Gpu-based ising computing for solving max-cut combinatorial optimization problems, Integration **69**, 335 (2019).
[19] J. Chou, S. Bramhavar, S. Ghosh, and W. Herzog, Analog Coupled Oscillator Based Weighted Ising Machine, Sci Rep **9**, 14786 (2019).
[20] W. Moy, I. Ahmed, P.-w. Chiu, J. Moy, S. S. Sapatnekar, and C. H. Kim, A 1,968-node coupled ring oscillator circuit for combinatorial optimization problem solving, Nat Electron **5**, 310 (2022).
[21] T. Wang and J. Roychowdhury, OIM: Oscillator-based Ising Machines for Solving Combinatorial Optimisation Problems 10.48550/ARXIV.1903.07163 (2019).
[22] T. Wang and J. Roychowdhury, Oscillator-based Ising Machine 10.48550/ARXIV.1709.08102 (2017).
[23] G. Csaba and W. Porod, Coupled oscillators for computing: A review and perspective, Applied Physics Reviews **7**, 011302 (2020).
[24] C. Bybee, D. Kleyko, D. E. Nikonov, A. Khosrowshahi, B. A. Olshausen, and F. T. Sommer, Efficient optimization with higher-order ising machines (2022), arXiv:2212.03426 [cs.ET].
[25] K. Ochs, B. Al Beattie, and S. Jenderny, An ising machine solving max-cut problems based on the circuit synthesis of the phase dynamics of a modified kuramoto model, 2021 IEEE International Midwest Symposium on Circuits and Systems (MWSCAS) , 982 (2021).
[26] I. Ahmed, P.-W. Chiu, W. Moy, and C. H. Kim, A Probabilistic Compute Fabric Based on Coupled Ring Oscillators for Solving Combinatorial Optimization Problems, IEEE J. Solid-State Circuits **56**, 2870 (2021).
[27] Y. Zhang, Y. Deng, Y. Lin, Y. Jiang, Y. Dong, X. Chen, G. Wang, D. Shang, Q. Wang, H. Yu, and Z. Wang, Oscillator-network-based ising machine, Micromachines **13**, 10.3390/mi13071016 (2022).
[28] R. Hamerly, T. Inagaki, P. L. McMahon, D. Venturelli, A. Marandi, T. Onodera, E. Ng, C. Langrock, K. Inaba, T. Honjo, K. Enbutsu, T. Umeki, R. Kasahara, S. Utsunomiya, S. Kako, K.-i. Kawarabayashi, R. L. Byer, M. M. Fejer, H. Mabuchi, D. Englund, E. Rieffel, H. Takesue, and Y. Yamamoto, Experimental investigation of performance differences between coherent Ising machines and a quantum annealer, Sci. Adv. **5**, eaau0823 (2019).
[29] M. Calvanese Strinati, L. Bello, E. G. Dalla Torre, and A. Pe'er, Can Nonlinear Parametric Oscillators Solve Random Ising Models?, Phys. Rev. Lett. **126**, 143901 (2021).
[30] T. L. Heugel, O. Zilberberg, C. Marty, R. Chitra, and A. Eichler, Ising machines with strong bilinear coupling, Phys. Rev. Res. **4**, 013149 (2022).
[31] L. English, A. Zampetaki, K. Kalinin, Berloff, N.G., and P. Kevrekidis, An ising machine based on networks of subharmonic electrical resonators, Communications Physics **5** (2022).
[32] L. Bello, M. Calvanese Strinati, E. G. Dalla Torre, and A. Pe'er, Persistent coherent beating in coupled parametric oscillators, Phys. Rev. Lett. **123**, 083901 (2019).
[33] M. Calvanese Strinati, I. Aharonovich, S. Ben-Ami, E. G. Dalla Torre, L. Bello, and A. Pe'er, Coherent dynamics in frustrated coupled parametric oscillators, New J. Phys. **22**, 085005 (2020).
[34] T. Feng, Q. Yuan, D. Yu, B. Wu, and H. Wang, Concepts and Key Technologies of Microelectromechanical Systems Resonators, Micromachines **13**, 2195 (2022).
[35] G. Pillai and S.-S. Li, Piezoelectric MEMS Resonators: A Review, IEEE Sensors J. **21**, 12589 (2021).
[36] M. J. Bereyhi, A. Arabmoheghi, A. Beccari, S. A. Fedorov, G. Huang, T. J. Kippenberg, and N. J. Engelsen, Perimeter Modes of Nanomechanical Resonators Exhibit Quality Factors Exceeding 10ˆ9 at Room Temperature, Phys. Rev. X **12**, 021036 (2022), publisher: American Physical Society.
[37] C. Cassella, Y. Hui, Z. Qian, G. Hummel, and M. Rinaldi, Aluminum Nitride Cross-Sectional Lamé Mode Resonators, J. Microelectromech. Syst. **25**, 275 (2016).
[38] See Supplemental Material [URL by Editorial Staff] for details on the analytical treatment of PFDs as MRs, the design and simulation of PFDs, the comparison of PFDs with other parametrons, the computational principle of coupled PFDs, the impact of annealing on the performance of PFD IMs, and the adopted experimental setup and results. The Supplemental Material also includes Refs. [58-63].
[39] J. A. Acebrón, L. L. Bonilla, C. J. Pérez Vicente, F. Ritort, and R. Spigler, The kuramoto model: A simple paradigm for synchronization phenomena, Rev. Mod. Phys. **77**, 137 (2005).
[40] H. M. E. Hussein, M. Rinaldi, M. Onabajo, and C. Cassella, A chip-less and battery-less subharmonic tag for wireless sensing with parametrically enhanced sensitivity and dynamic range, Sci Rep **11**, 3782 (2021).
[41] H. M. E. Hussein, M. Rinaldi, M. Onabajo, and C. Cassella, Capturing and recording cold chain temperature violations through parametric alarm-sensor tags, Appl. Phys. Lett. **119**, 014101 (2021).
[42] H. M. E. Hussein, M. A. A. Ibrahim, M. Rinaldi, M. Onabajo, and C. Cassella, Reflective Parametric Frequency-Selective Limiters With Sub-dB Loss and microWatts Power Thresholds, IEEE Transactions on Microwave Theory and Techniques **69**, 2989 (2021).
[43] F. Ramirez, R. Melville, A. Suarez, and J. S. Kenney, Nonlinear analysis and design of frequency selective limiters based on parametric circuits, in *2008 IEEE*

MTT-S International Microwave Symposium Digest (2008) pp. 947–950.

[44] L. G. Villanueva, R. B. Karabalin, M. H. Matheny, E. Kenig, M. C. Cross, and M. L. Roukes, A Nanoscale Parametric Feedback Oscillator, Nano Letters **11**, 5054 (2011).

[45] C. Cassella, S. Strachan, S. W. Shaw, and G. Piazza, Phase noise suppression through parametric filtering, Applied Physics Letters **110**, 063503 (2017).

[46] H. M. E. Hussein, M. A. A. Ibrahim, G. Michetti, M. Rinaldi, M. Onabajo, and C. Cassella, Systematic Synthesis and Design of Ultralow Threshold 2:1 Parametric Frequency Dividers, IEEE Trans. Microwave Theory Techn. **68**, 3497 (2020).

[47] N. Casilli, O. Kaya, T. Kaisar, B. Davaji, P. X.-L. Feng, and C. Cassella, Nonvolatile state configuration of nanowatt parametric Ising spins through ferroelectric hafnium zirconium oxide mems varactors, in *2023 IEEE 36th International Conference on Micro Electro Mechanical Systems (MEMS)* (2023) pp. 511–514.

[48] J. F. Rhoads, S. W. Shaw, K. L. Turner, J. Moehlis, B. E. DeMartini, and W. Zhang, Generalized parametric resonance in electrostatically actuated microelectromechanical oscillators, Journal of Sound and Vibration **296**, 797 (2006).

[49] M. Kumar and P. Varshney, Numerical simulation of van der pol equation using multiple scales modified lindstedt–poincare method, Proc. Natl. Acad. Sci., India, Sect. A Phys. Sci. **91**, 55 (2020).

[50] M. Calvanese Strinati, L. Bello, A. Pe'er, and E. G. Dalla Torre, Theory of coupled parametric oscillators beyond coupled Ising spins, Phys. Rev. A **100**, 023835 (2019).

[51] J. Wang, D. Ebler, K. Wong, D. Hui, and J. Sun, Bifurcation behaviors shape how continuous physical dynamics solves discrete ising optimization, Nature Communications 10.1038/s41467-023-37695-3 (2023).

[52] J. Roychowdhury, A global lyapunov function for the coherent ising machine, Nonlinear Theory and Its Applications, IEICE **13**, 227 (2022).

[53] R. F. Pierret, *Advanced semiconductor fundamentals*, 2nd ed., Modular series on solid state devices No. v. 6 (Prentice Hall, Upper Saddle River, N.J, 2003).

[54] M. Calvanese Strinati, D. Pierangeli, and C. Conti, All-optical scalable spatial coherent ising machine, Phys. Rev. Appl. **16**, 054022 (2021).

[55] T. Kaisar, S. M. E. H. Yousuf, J. Lee, A. Qamar, M. Rais-Zadeh, S. Mandal, and P. X.-L. Feng, Five low-noise stable oscillators referenced to the same multimode AlN/Si mems resonator, IEEE Transactions on Ultrasonics, Ferroelectrics, and Frequency Control **70**, 1213 (2023).

[56] T. Albash, V. Martin-Mayor, and I. Hen, Analog errors in ising machines, Quantum Sci. Technol. **4** (2019).

[57] T. Leleu, Y. Yamamoto, P. L. McMahon, and K. Aihara, Destabilization of local minima in analog spin systems by correction of amplitude heterogeneity, Phys. Rev. Lett. **122**, 040607 (2019).

[58] A. Suarez, *Analysis and Design of Autonomous Microwave Circuits* (Wiley, Hoboken, NJ, USA, 2009).

[59] C. Cassella and G. Piazza, Low phase-noise autonomous parametric oscillator based on a 226.7 MHz AlN contour-mode resonator, IEEE Trans. Ultrason. Ferroelect. Freq. Contr. **62**, 617 (2015).

[60] M. Roberg and C. Campbell, A novel even and odd-mode symmetric circuit decomposition method, in *2013 IEEE Compound Semiconductor Integrated Circuit Symposium (CSICS)* (2013) pp. 1–4.

[61] Z. Wang, A. Marandi, K. Wen, R. L. Byer, and Y. Yamamoto, Coherent Ising machine based on degenerate optical parametric oscillators, Phys. Rev. A **88** (2013).

[62] F. Böhm, T. V. Vaerenbergh, G. Verschaffelt, and G. Van der Sande, Order-of-magnitude differences in computational performance of analog Ising machines induced by the choice of nonlinearity, Commun. Phys. **4** (2021).

[63] M. Nifle and H. J. Hilhorst, New critical-point exponent and new scaling laws for short-range ising spin glasses, Phys. Rev. Lett. **68**, 2992 (1992).